SuperDARN observations of the two component model of ionospheric convection

A. Grocott[1], M.-T. Walach[1], S. E. Milan[2]

[1]Lancaster University, Lancaster, LA1 4YB, U.K.
[2]University of Leicester, Leicester, LE1 7RH, U.K.

Key Points:

- A dependence of the local time of the dawn and dusk convection cell foci on IMF strength and geomagnetic activity is observed
- This provides supporting evidence for the two components of ionospheric convection predicted by the expanding contracting polar cap model
- These results were obtained using a 20 year archive of Super Dual Auroral Radar Network (SuperDARN) observations of the convection

Corresponding author: Adrian Grocott, a.grocott@lancaster.ac.uk

Abstract

We use a 20 year database of Super Dual Auroral Radar Network (SuperDARN) observations to investigate the two component model of ionospheric convection. A convection pattern is included in the database if it is derived from at least 250 radar vectors and has a distribution of electric potential consistent with Dungey-cycle twin vortex flow (a negative potential peak in the dusk cell and a positive potential peak in the dawn cell). We extract the locations of the foci of the convection cells from the SuperDARN convection patterns, and compare their dependencies on the north-south component of the interplanetary magnetic field, IMF B_Z, and the auroral electrojet index, AL. We define a quantity, $dMLT$, as the hour angle between the dawn and dusk convection cell foci, which we use as a proxy for the extent to which the dayside or nightside component of the convection pattern is dominating. We find that at a fixed level of AL, $dMLT$ decreases with increasingly negative IMF B_Z, consistent with an increasing dominance of dayside reconnection. We also find that at a fixed level of IMF B_Z, $dMLT$ increases with increasingly negative AL, consistent with an increasing dominance of nightside reconnection, but only up to modest values of AL (to $\sim -200\,\mathrm{nT}$). As AL becomes further enhanced $dMLT$ decreases again, which we attribute to an inherent dependence of AL on IMF B_Z.

Plain Language Summary

The Earth's upper atmosphere is coupled to the near-Earth space environment – the magnetosphere – via the planet's magnetic field. This magnetic coupling drives a circulation of plasma – the electrically charged component of the atmosphere, called the ionosphere – from day to night across the poles and back again at lower latitudes. This circulation of plasma is a key component of the energy transport in the magnetosphere-ionosphere system. The circulation is not steady, instead changing in strength whilst expanding and contracting due to the time-dependence of the driving mechanisms. To understand these mechanisms we can model the ionospheric circulation and test the models with observations. In this paper we use a 20 year database of ionospheric radar observations of the plasma flow to test one such model – the expanding-contracting polar cap (ECPC) model – and find evidence to support its predictions of separate dayside and nightside components of the flow.

1 Introduction

The expanding contracting polar cap (ECPC) model of ionospheric convection (Cowley & Lockwood, 1992) dictates that transpolar flow (and hence voltage) should be excited when magnetic reconnection changes the topology of the Earth's magnetic field. Dayside reconnection, between the interplanetary magnetic field (IMF) in the solar wind and the Earth's magnetic field opens previously closed terrestrial field lines, appending newly open flux to the magnetopause, which is then carried into the polar cap by an enhanced plasma flow (e.g. Etemadi et al., 1988; Greenwald et al., 1999). Nightside reconnection, between the open field lines of the northern and southern magnetotail lobes, closes previously open field lines which are carried out of the polar cap and back to the dayside by a similar excitation of plasma flows (e.g. Grocott et al., 2002; Gordeev et al., 2011). The ECPC model describes the basic form that the ionospheric convection cells should take during intervals of dominant dayside or nightside reconnection as illustrated in, for example, Figure 2 of Lockwood and McWilliams (2021). According to the model, when dayside reconnection is dominant the foci of the twin-vortex convection cells are expected to be displaced towards the dayside and when nightside reconnection is dominant the foci of the twin-vortex convection cells are expected to be displaced towards the nightside.

The idea that solar wind - magnetosphere coupling drives magnetospheric and ionospheric convection is not disputed. It is relatively straightforward to show that the strength of the ionospheric convection (e.g. MacDougall & Jayachandran, 2001) or transpolar voltage, V_{PC} (e.g. Boyle et al., 1997) is related to the concurrent solar wind and IMF conditions. Difficulties arise in isolating the separate contributions from dayside and, in particular, nightside reconnection. Whilst dayside reconnection rates are simple to estimate from upstream solar wind and IMF observations (e.g. Milan et al., 2012), dayside driving tends to precipitate nightside reconnection. Statistical results, such as those of Boyle et al. (1997) and larger-scale models of convection (e.g. Greenwald et al., 1996; Ruohoniemi & Greenwald, 2005; Weimer, 2005; Thomas & Shepherd, 2018) therefore tend to reveal a somewhat steady-state approximation to the response to solar wind driving.

Isolating and quantifying the nightside reconnection contribution is a particular challenge, owing in part to a difficulty in measuring the nightside reconnection rate, or estimating it from in-situ observations. In a study of transpolar voltage data from the Super Dual Auroral Radar Network (SuperDARN) Lockwood and McWilliams (2021) used the AL magnetic index as a proxy for the nightside reconnection rate. They used hourly means to show that V_{PC} increases both for increasingly negative IMF B_Z, and increasingly negative AL index, consistent with both dayside and nightside reconnection being responsible for driving convection, as predicted by the ECPC model. A difficulty in interpreting this result arises from the fact that taking hourly averages significantly smoothes structures in the data, especially high values, since V_{PC} is not normally distributed. It is also the case that AL and IMF B_Z are not independent; intervals of strongly negative IMF B_Z correlate with intervals of enhanced AL index. Lockwood and McWilliams (2021) attempt to mitigate this by considering that V_{PC} increases with increasing strength of AL index even for a fixed value of IMF B_Z. However, this does not account for the possibility that factors additional to IMF B_Z strength may directly affect the dayside reconnection rate (e.g. Borovsky et al., 2008).

In this paper we use a 20 year archive of SuperDARN radar data to provide direct evidence for the two component model of ionospheric convection. We locate the convection cell foci in the SuperDARN observations and investigate the statistics of their location, in the context of the transpolar voltage, solar wind and geomagnetic observations. For simplicity, and in order to make direct comparisons with the findings of Lockwood and McWilliams (2021), we use IMF B_Z and the AL index as proxies for the strength of dayside and nightside reconnection. We find that significant voltages may be driven for both dayside and nightside displaced convection cell foci. The foci tend to be displaced towards the dayside when IMF B_Z is negative and AL small. They tend to be displaced towards the nightside when IMF B_Z is positive and AL modest. The dawn and dusk cell foci do not appear to respond in the same way to differing driving conditions, making the overall behaviour of the convection patterns non-trivial to interpret.

2 Data Analysis

Large-scale observations of ionospheric convection from 1999-2018 are provided by the Super Dual Auroral Radar Network (SuperDARN). SuperDARN is an international array of HF ionospheric radars located in the polar regions of both hemispheres whose fields-of-view cover much of the polar, auroral and subauroral regions. Each radar measures the line-of-sight (LOS) Doppler velocity of ionospheric plasma irregularities from which the radars scatter (Greenwald et al., 1995; Chisham et al., 2007). The radars scan through typically 16 beams (look directions) making observations at typically 75 locations along each beam at between 180 km and over 3500 km in range. The LOS velocities are derived from best fit autocorrelation functions of the backscattered radar signals. To produce large-scale convection maps, the line-of-sight velocities are median filtered at 2-min cadence onto an equal area polar grid of cell size $\sim 110 \times 110$ km. The latitudinal extent of the convection is determined by fitting a 'Heppner-Maynard' bound-

ary to the gridded velocities (see Heppner & Maynard, 1987; Shepherd & Ruohoniemi, 2000). A best-fit spherical harmonic expansion of the ionospheric electric potential is then derived from the radar data (Ruohoniemi & Baker, 1998). Information from a statistical convection model (Thomas & Shepherd, 2018), parameterised by IMF conditions, is used to supplement the radar observations to ensure sufficient coverage of data for the spherical harmonic fit to converge. Full details of the convection mapping software are provided by the SuperDARN Data Analysis Working Group et al. (2018) with the processing steps followed in this study being detailed in Walach et al. (2022).

From our convection map archive we extract the magnetic latitude and magnetic local time (MLT) of the peaks of the positive and negative electric potential. We then impose a number of criteria by which we reduce the data set. We first remove any maps for which the total number of gridded radar vectors, n, is less than 250. This criterion removes maps which are more likely to be dominated by the statistical convection model used in the fitting. Similar thresholds have been employed in previous studies (e.g. Imber et al. (2013) used $n > 200$, Lockwood and McWilliams (2021) used $n > 255$, and Fogg et al. (2020) used $n > 400$). A sensitivity test of our results to the choice of n (not shown) suggests no significant difference when using $n > 250$. We then impose the condition that the MLT of the positive potential peak be less than 12 h, and that the MLT of the negative potential peak be greater than 12 h. This is done to maximise the likelihood that the positive and negative potential peaks identified correspond, respectively, to the foci of the dawn and dusk Dungey-cycle twin vortex convection cells. The resulting data set is then further subdivided by concurrent IMF conditions and geomagnetic activity levels as discussed in the following section. IMF data are provided by the Magnetic Fields Experiment (Smith et al., 1998) on board the Advanced Composition Explorer (ACE) spacecraft (Stone et al., 1998) and geomagnetic activity indices are described by Davis and Sugiura (1966).

3 Results

Figure 1 presents an overview of the convection cell foci statistics. All panels are presented in magnetic latitude, magnetic local time coordinates, with a grid cell size of 1 h of local time and 5° of latitude. Overlaid on each panel for reference is a model kp=2 Feldstein and Starkov (1967) oval. In panel (a) we show the full distribution of the data set which, after the filtering outlined in section 2, contains over 400,000 convection maps ($\sim 8\%$ of the total). A wide range of cell foci locations exist, with 96% of dusk foci (and 98% of dawn foci) lying in the latitude range $70° - 85°$, and 97% of dusk foci (95% of dawn foci) lying in the MLT range 14 - 22 h (2 - 10 h).

Figure 1b-c show subsets of the data after filtering for conditions of IMF B_Z and AL index expected to yield dominant (b) dayside and (c) nightside reconnection. In panel (b) the data have been filtered to include only instances of negative IMF $B_Z < -2$ nT and small $AL > -5$ nT. In panel (c) the data have been filtered to include only instances of strongly positive IMF $B_Z > 4$ nT and modest $-50 > AL > -150$ nT. The reasons for this choice of filter parameter values is discussed in detail below. In panel (b) we can see that the range of foci latitudes and local times has been reduced compared to the full data set in panel (a). The foci in (b) tend to be limited to higher latitudes, indicative of a smaller polar cap. Although the distribution of foci locations spans the dusk-dawn meridian both to the dayside and nightside, there is a slight tendency towards the dayside with 57% of dawnside foci and 59% of duskside foci being located closer to noon than to midnight. In panel (c) we can see that the foci tend to be at lower latitudes than in panel (b). Although the foci local times stil exhibit some spread, they are more often located on the nightside, with 79% of dawnside foci and 77% of duskside foci located closer to midnight than to noon.

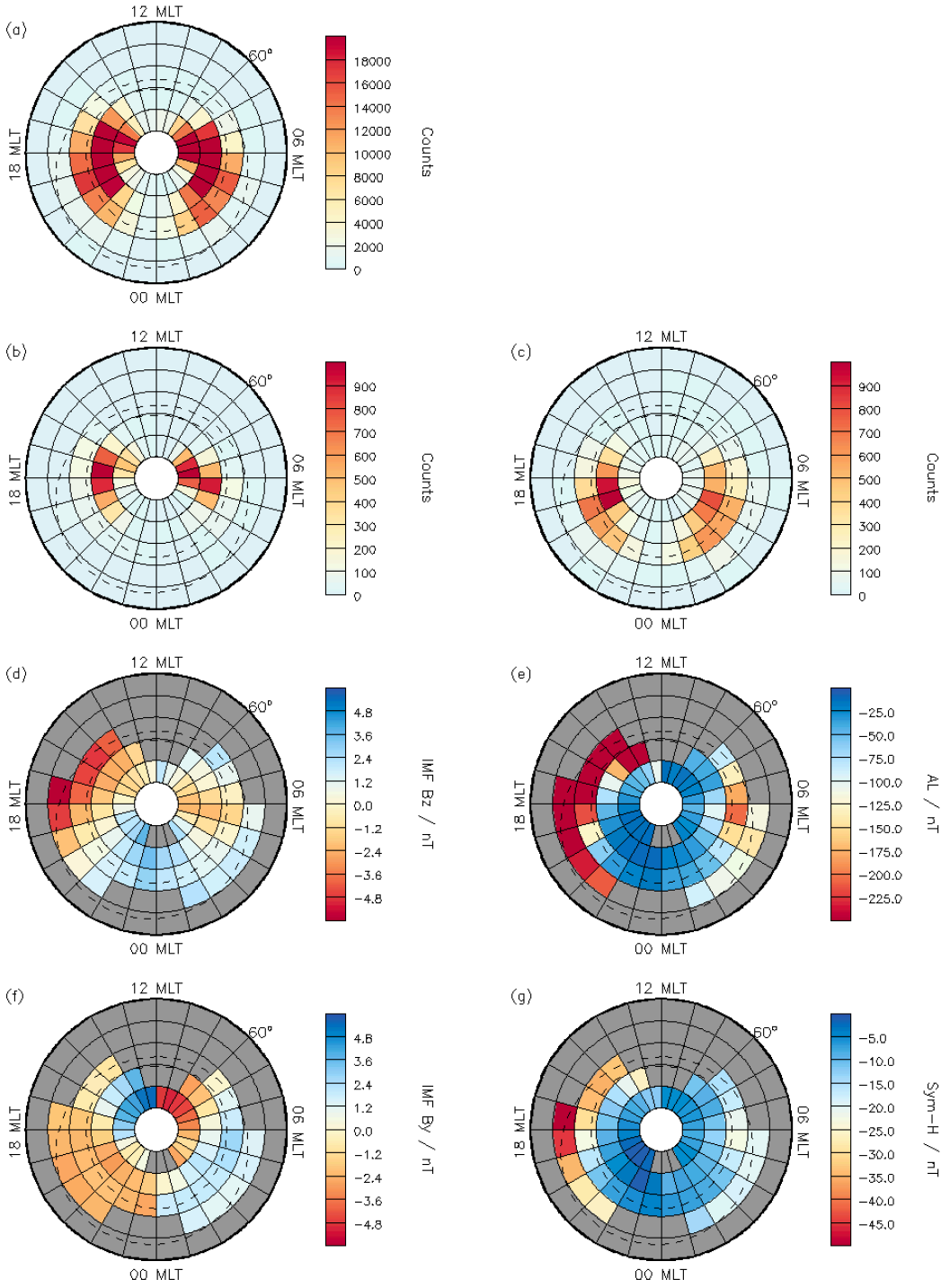

Figure 1. Distributions of the convection cell foci presented in a magnetic latitude, magnetic local time grid, with a model kp=2 Feldstein and Starkov (1967) oval shown for reference. (a) the distribution of all dusk and dawn cell foci included in the data set, (b) and (c) subsets of (a) that have been subject to filtering based on IMF Bz and *AL* to correspond to expected intervals of dominant reconnection on the dayside and nightside, respectively, (d) - (g) median parameters in each grid cell of panel (a): (d) IMF Bz, (e) AL, (f) IMF By, (g) Sym-H (cells containing fewer than 500 values are shaded grey).

Figure 1d-g presents four examples of how the convection cell foci might exhibit a dependency on the IMF and geomagnetic activity. In each panel, the data set from panel (a) is now colour-coded to the median value in each grid cell of (d) IMF B_Z, (e) AL index, (f) IMF B_Y and (g) Sym-H index. To minimise the effect of small statistics unduly influencing the results we colour cells containing fewer than 500 values grey. Panel (d) indicates that, for the dusk cell in particular, strongly negative B_Z favours lower-latitude, dayside convection cell foci, with positive B_Z favouring nightside foci. Any dawn cell focus dependency is less apparent. Cells close to dawn generally correspond to weakly negative B_Z and cells nearer to midnight weakly positive B_Z, but there is also a population of cells closer to noon corresponding to weakly positive B_Z. Panel (e) suggests that when AL is more strongly negative, the convection cell foci (and hence polar cap boundary) tends to be at lower latitudes. However, there is no clear tendency for more nightside located foci at more negative AL values. Panel (f) reveals an IMF B_Y-dependent rotation of the convection pattern, with positive B_Y producing a clockwise rotation (dusk foci closer to noon and dawn foci closer to midnight) and negative B_Y producing an anticlockwise rotation (dusk foci closer to midnight and dawn foci closer to noon), but with no tendency for both foci to be closer to either noon or midnight. Lastly, panel (g) shows that the foci latitude decreases with increasingly negative Sym-H, with no obvious correlation with the foci local times.

The data presented in Figure 1 are suggestive of a dependence of the foci local times on IMF and geomagnetic activity, but also of the specifics of that dependence being non-trivial. In Figure 2 we therefore explore this dependence in more detail. Figure 2a-b show, respectively, the distributions of the dawn and dusk convection cell foci local times (which we henceforth refer to as CCFLT for brevity). In each case the CCFLT data are plotted versus AL and IMF B_Z, with cells containing fewer than 30 values omitted. The first thing to note is that there is an interdependence of AL and B_Z, with strongly positive B_Z only occurring for weak or positive AL and strongly negative AL only occurring for negative B_Z. This inherently limits the possible dependencies of the CCFLT on the two parameters. At modest levels of AL there is a clear dependence of the CCFLT on B_Z. The dawn CCFLT moves from being located close to dawn for negative B_Z into the predawn sector for positive B_Z. Likewise, the dusk CCFLT moves from being located close to dusk for negative B_Z to the postdusk sector for positive B_Z. The dawn CCFLT shows very little dependence on AL. There is some indication that at the weaker (positive) end of the AL range the CCFLT are slightly shifted towards the dayside. This would be consistent with weak or positive AL being indicative of a lack of nightside reconnection, but negative of about $-50\,\mathrm{nT}$ there is little further discernible trend. The dusk CCFLT seem to respond more to changes in AL. Moving from weak (positive) AL to more strongly negative AL the CCFLT tend to move towards the dayside. This is counter to what is expected, if increasingly negative AL was indicative of more dominant nightside reconnection.

In Figure 2c we attempt to combine the information about the dusk and dawn CCFLT into a single parameter, to quantify the extent to which the foci are closer to the dayside or nightside. We define a quantity $dMLT$ which is the hour angle, or difference in hours of local time, between the dusk and dawn cell foci, or $CCFLT_{dusk} - CCFLT_{dawn}$, such that $dMLT = 12\,\mathrm{h}$ corresponds to convection cell foci that lie along a meridian line. This might be the dawn-dusk meridian or, if the convection pattern is rotated about the pole, then one cell's focus would be displaced towards noon to the same extent that the others cell's focus was displaced towards midnight. Values of $dMLT < 12\,\mathrm{h}$ then represents a convection pattern where the CCFLTs are offset towards the dayside, or at least, where one cell's focus is displaced towards noon to a greater extent than the other's is displaced towards midnight. Similarly, $dMLT > 12\,\mathrm{h}$ represents a convection pattern where the CCFLTs are offset towards the nightside, or at least, where one cell's focus is displaced towards midnight to a greater extent than the other's is displaced towards noon.

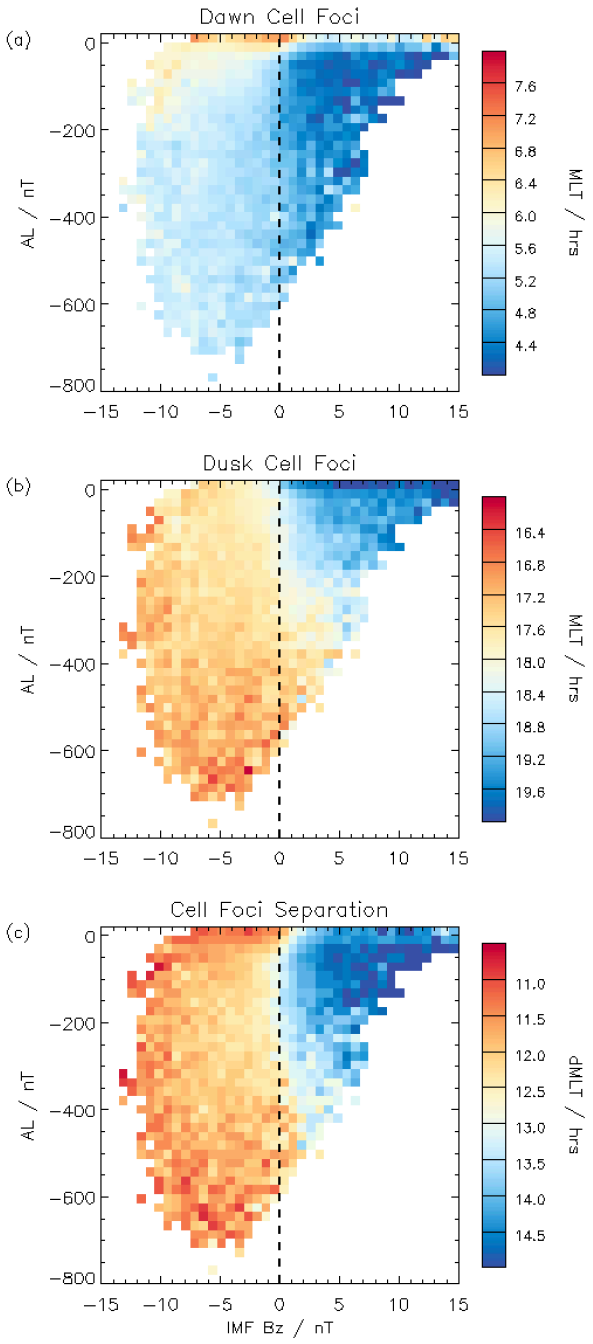

Figure 2. Distributions of the convection cell foci magnetic local times plotted versus AL and IMF B_Z for (a) the dawn cell and (b) the dusk cell. (c) hours of separation of the dawn and dusk cells, $dMLT$. Cells containing fewer than 30 values are omitted.

Figure 2c shows that for the majority of negative IMF B_Z and AL conditions, the CCFLT separation, $dMLT$, is close to 12 h. When AL is weak and B_Z negative, $dMLT$ is less than 12 h. This informed our choice of IMF $B_Z < -2$ nT and $AL > -5$ nT for our dayside reconnection filter. As AL becomes increasingly negative, up to ~ -400 nT, so B_Z must be increasingly negative for $dMLT$ to remain less than 12 h. For AL index below ~ -400 nT, however, it appears that $dMLT$ becomes less sensitive to B_Z, with $dMLT$ remaining less than 12 h for increasingly weaker B_Z. For AL index below ~ -600 nT it appears that $dMLT$ may be less than 12 h for any value of negative B_Z. When B_Z is positive, $dMLT$ is almost always greater than 12 h, with the largest values occurring for $B_Z > 4$ nT and $-50 > AL > -150$ nT. This informed our choice of nightside reconnection filter. As AL becomes increasingly negative below ~ -200 nT, $dMLT$ decreases.

In Figure 3 we inspect the behaviour of $dMLT$ in more detail. In (a) we show the variation of V_{PC} with $dMLT$ and in (b) we show probability distributions of the $dMLT$ data subsets. The vertical dashed line in both panels marks $dMLT = 12$ h. The distribution of V_{PC} appears to be multimodal, with major peaks at $dMLT \sim 11$ h and $dMLT \sim 13$ h and with a local minimum at 12 h. At the same time, the highest V_{PC} values occur for $dMLT$ values close to 12 h. For earlier and later $dMLT$ values, the peak V_{PC} values decrease. Dayside driving seems to be limited to a small range of $dMLT$, whereas nightside dMLT values occur over a wider range. In particular, a second small population of weaker V_{PC} exists at large $dMLT$ values of $\sim 16 - 18$ h.

The distribution of $dMLT$ values for the full data set from Fig.1a is shown as a dashed black line in Figure 3b. This is consistent with the broad nature of the distributions of CCFLT. Shown in red is the distribution of the data subset from Fig.1b filtered for dominant dayside reconnection. The distribution is somewhat narrower, and is shifted to smaller dMLT, consistent with the cell foci being closer to the dayside. Shown in blue is the distribution of the data subset from Fig.1c filtered for dominant nightside reconnection. This distribution is still quite broad, and does overlap with the dayside distribution, but is overall shifted to larger dMLT, consistent with the cell foci being closer to the nightside.

In Figure 4 we explore whether the overlap between the dayside and nightside reconnection filtered $dMLT$ values is reflected in the separate dawn and dusk CCFLTs, or whether individually they form discrete populations. Panel (a) presents the the full data set from Fig. 1a, with the dusk CCFLT plotted against the dawn CCFLT. This shows that, whilst the dusk cell focus is found with similar prevalence in the afternoon (47%) and evening (53%) sectors, the dawn cell focus is less often located on the dayside (35%), being more often predawn (65%). An intrinsic asymmetry is apparent in the foci locations, in that the most populous quadrant of the distribution is pre-dawn/pre-dusk (33%), consistent with a clockwise rotation of the convection pattern. This compares to only 21% in the post-dawn/post-dusk quadrant that corresponds to an anticlockwise rotation. The post-dawn/pre-dusk quadrant (dayside foci) contains just 14% of the data, whereas the pre-dawn/post-dusk quadrant (nightside foci) contains 32% of the data.

In Figure 4b-c we show similar plots for the (b) dayside and (c) nightside reconnection filtered subsets from Fig.1b and c. The nightside subset (panel c) clearly shows the expected behaviour, with 60% of the data located in the pre-dawn/post-dusk quadrant (corresponding to $dMLT > 12$ h) and only 5% in the post-dawn/pre-dusk quadrant (corresponding to $dMLT < 12$ h). The behaviour of the dayside subset (panel b) is less clear cut, with only 30% in the post-dawn/pre-dusk quadrant. A similar proportion of this subset (31%) is in the pre-dawn/pre-dusk quadrant, similar to panel (a). This is consistent with the absence of any significant dawn CCFLT > 6 h for any combination of B_Z or AL as noted in reference to Fig. 2. Nevertheless, it is very much apparent that the dayside subset is quite distinct from the nightside subset, with only 14%

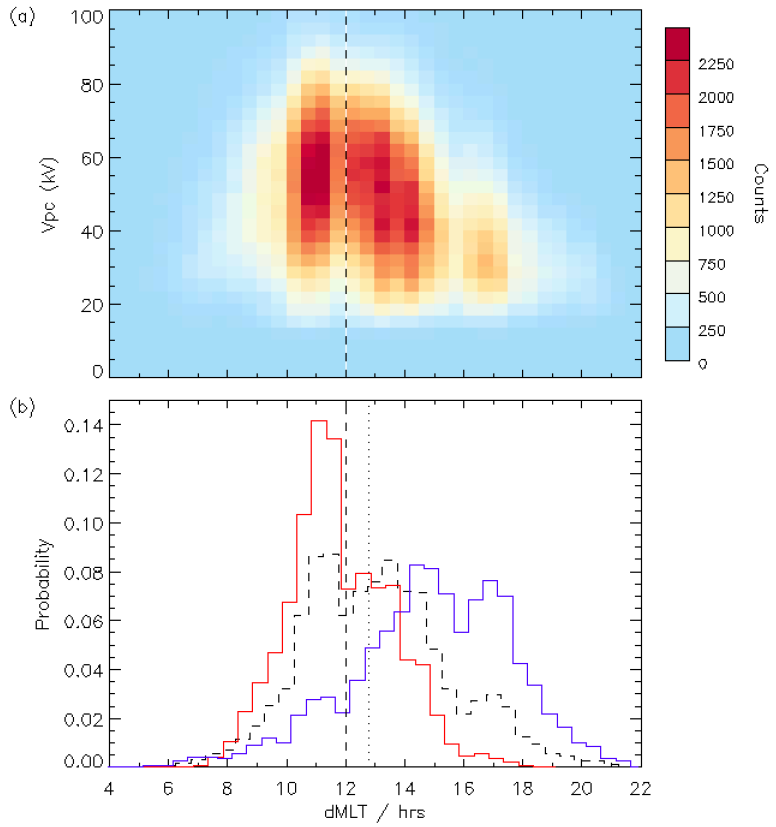

Figure 3. Probability distributions of the dawn-dusk foci separation, $dMLT$. The full data set from Fig.1a is shown as a black dashed line and the filtered data sets from Fig.1b and c are shown by the solid red (dayside) and blue (nightside) lines, respectively. The vertical dashed line marks 12 MLT. The vertical dotted line marks the mean $dMLT = 12.8$ h.

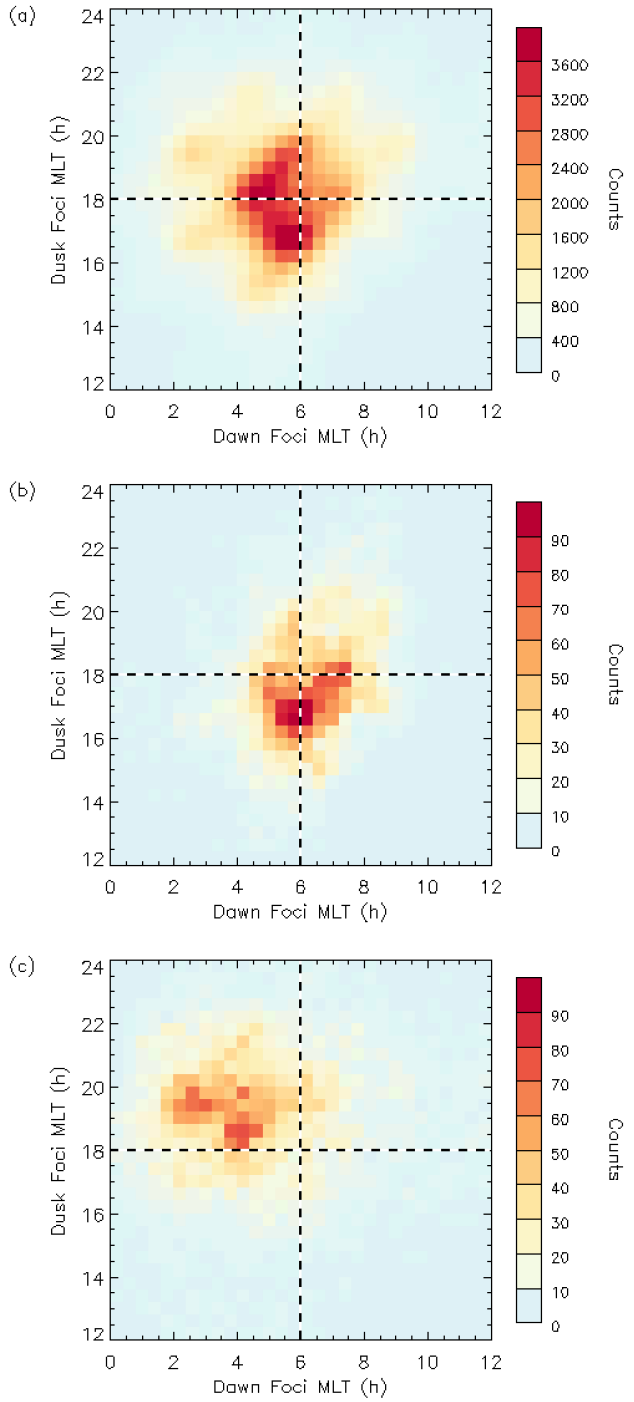

Figure 4. Occurrence distributions of coincident dawn and dusk convection cell foci magnetic local times. (a) the full data set from Fig.1a, (b) and (c) the filtered data sets from Fig.1b and c, respectively.

in the pre-dawn/post-dusk (nightside) quadrant where most of the nightside subset is located.

4 Discussion

The primary aim of this study was to determine whether the two-component model of ionospheric convection predicted by the ECPC model is apparent in SuperDARN ionospheric convection observations. Using the locations of the peaks in electric potential as proxies for the convection cell foci, we have presented statistics of the locations of the foci from which we can draw a number of conclusions. Firstly, as shown in Figure 1a, the distribution of foci locations is revealed by the SuperDARN data to be quite wide, despite our pre-selection criteria for the foci having reduced the data to 8% of the total available. The spread of latitudes of the foci indicate a range of polar cap sizes and the spread of local times is consistent with convection being driven from both the dayside and nightside. In order to isolate the convection patterns associated with dominant dayside and nightside reconnection we have inspected the dependence of the locations of the convection cell foci on a number of parameters. It is apparent from Figure 1d-e, however, that no single parameter can explain the observations.

Figure 1d suggests that IMF B_Z does exhibit some control, being more positive for foci locations on the nightside. This is consistent with the idea that the Dungey cycle can be maintained even during intervals of positive IMF B_Z, but that dayside low-latitude reconnection will be inactive, or at a low enough rate that nightside reconnection will be dominant (e.g. Grocott et al., 2002, 2003). When B_Z is negative, and the dayside reconnection rate is high, we might expect the foci to be located on the dayside. This seems to be the case for the dusk cell, but appears not to be the case for the dawn cell, for which moderately negative B_Z correspond to foci being located close to dawn. The lower magnitude of the B_Z averages on the dawn side also suggests that the dawn cell location is less strongly correlated with B_Z. We consider this apparent dawn - dusk asymmetry further, below.

Figure 1e shows a dependence of the foci locations on the AL index. In this case, the dependence appears to more strongly control the latitude of the foci, with AL being of lower magnitude for higher latitude foci and larger magnitude for lower latitude foci. There is little evidence that the AL index alone has any influence on the local time of the foci. This relationship is very similar to the relationship with Sym-H shown in panel (g). Sym-H is a proxy for the ring current strength (Iyemori, 1990) and as such is a more global measure of geomagnetic activity that will tend to be high when the polar cap is expanded and both dayside and nightside reconnection are active (e.g. Walach & Grocott, 2019), although there is some evidence that nightside reconnection may be suppressed on shorter timescales when Sym-H is high (e.g. Nakai & Kamide, 2003; Milan et al., 2008). That the pattern of AL index resembles the Sym-H pattern is indicative of an inherent dependence of AL on B_Z, certainly on average and, as we discuss below, even on much shorter timescales, such that increasingly negative AL is always more likely for increasingly negative IMF B_Z. This suggests that although nightside reconnection is expected to become enhanced with increasingly negative AL, it does so in response to enhanced dayside reconnection. This coupled nature of the nightside and dayside reconnection serves to complicate efforts to disentangle the contribution of each to the ionospheric convection pattern.

To better understand the interdependency of the AL index and IMF B_Z we presented in Figure 2a-b the distributions of the dawn and dusk convection cell foci local times (CCFLTs), respectively, with respect to AL and B_Z. These data revealed a degree of complexity in the relationships and we comment on a few key findings here. First, the differing behaviour of the dawn and dusk cell foci is readily apparent. The dusk cell focus is less often on the nightside and, contrary to expectations that enhanced (nega-

tive) AL should indicate dominant nightside reconnection, the focus is generally only on the nightside for weaker AL values above $\sim -200\,\mathrm{nT}$, and only if B_Z is also positive. When AL is more strongly negative, the dusk focus tends to be on the dayside. This is therefore more consistent with enhanced dayside reconnection and suggests that more elevated levels of nightside reconnection are themselves triggered by intervals of strong dayside reconnection, such that strongly negative AL is necessarily accompanied by negative B_Z and similar or even greater levels of dayside reconnection.

This tendency for strong AL to be often associated with an apparent absence of dominant nightside reconnection is also apparent in the $dMLT$ data in Figure 2c. For example, if we consider a fixed IMF B_Z value, e.g. $B_Z = 0$, we see that below $\sim -200\,\mathrm{nT}$, as AL becomes increasingly negative, $dMLT$ tends to decrease. This suggests either a weakening of nightside reconnection, or a strengthening of dayside reconnection. This appears contrary to the conclusion of Lockwood and McWilliams (2021) that an increase in V_{PC} with increasing AL magnitude at a fixed IMF B_Z was indicative of dominant nightside reconnection driving the convection. We suggest that this is a result of the intrinsic dependence of AL on B_Z, in that strong AL requires as a prerequisite strong dayside driving as well. This is consistent with the results of Milan et al. (2021) who studied the magnetospheric flux throughput in the Dungey cycle for a variety of convection states during the year 2010. We further suggest that considering a fixed value of, e.g., IMF B_Z is insufficient to ensure a fixed level of dayside driving. Otherwise an increased magnitude of AL ought not be associated with a smaller $dMLT$. This is further evidenced by considering that below AL values of $\sim -600\,\mathrm{nT}$ it appears that $dMLT < 12\,\mathrm{h}$ can occur for any value of negative B_Z. In other words, dayside driving must be high to produce such a large magnitude AL irrespective of the strength of IMF B_Z.

The upshot of this analysis is that the determination of suitable limits of IMF B_Z and AL index to be used as filters for intervals of dominant dayside and nightside reconnection is not straightforward. It seems that in general, the convection cell foci will be on the dayside for negative B_Z irrespective of AL. However, it is true that for modest AL, down to $\sim -200\,\mathrm{nT}$, the average $dMLT$ increases, presumably as a result of the contribution of nightside reconnection driven flows. The simplest way to ensure a predominance of dayside reconnection driven flows is thus to place a strict limit on the value of AL, and a such we have used $AL > -5\,\mathrm{nT}$. Determining similar limits to yield a predominance of nightside reconnection is more difficult. As noted above, high magnitude AL tends to require ongoing dayside driving, such that below values of $\sim -200\,\mathrm{nT}$ $dMLT$ tends to reduce. Nevertheless, some AL enhancement is required, or else $dMLT$ may be less than 12 h even for positive IMF B_Z. As negative B_Z will always produce a component of dayside reconnection driven flow, we thus opted for positive B_Z and modest negative AL as a filter for nightside reconnection dominated flow.

Returning then, to the distributions of foci locations, we now discuss the data subsets for dominant dayside or nightside reconnection driven flows shown in Figure 1b-c. The latitudes of the foci seem to vary as predicted by the ECPC model, being higher when we might expect dayside reconnection to dominate (Figure 1b), and being lower when we might expect nightside reconnection to dominate (Figure 1c). The reason for our expectations is based on the assumption that nightside reconnection only becomes significant once the polar cap has expanded, due to an accumulation of open flux. Prior to such an accumulation, when the polar cap will be smaller, we thus expect dayside reconnection to dominate. The expansion and contraction of the polar cap in association with dayside and nightside reconnection is not a new finding, having been demonstrated with respect to the substorm cycle in auroral (e.g. Milan et al., 2009), field-aligned current (e.g. Coxon et al., 2014) and convection data (e.g. Grocott et al., 2009), tested using radar observations (e.g. Walach et al., 2017; Sotirelis et al., 2017), and recently studied in detail over an extended interval by Milan et al. (2021). Here we simply note that the convection cell foci latitudes seem to obey the same basic behaviour.

The main focus of our analysis has concerned the local times of the convection cell foci. According to the ECPC model, as discussed theoretically by Cowley and Lockwood (1992), and later modelled numerically (e.g. Freeman & Morley, 2004; Lockwood & Morley, 2004; Lockwood et al., 2006; Milan et al., 2013; Walach et al., 2017), dayside and nightside reconnection each drive an independent component of the ionospheric convection pattern. The foci of the convection cells are expected to lie at the ends of the ionospheric projection of the reconnection line, hence, for dayside reconnection driven flow the foci are expected to be located on the dayside and for nightside reconnection driven flow the foci are expected to be located on the nightside. We see some evidence for this in Figure 1b-c, with the peaks of the foci distributions being located (just) on the dayside in Figure 1b and further round to the nightside in Figure 1c. The effect is perhaps clearer is the distributions of $dMLT$ shown in Figure 3b, in which the distributions of subsets filtered for dominant dayside and nightside reconnection are clearly separated. Nonetheless, significant overlap of the distributions is also apparent, suggesting that either our choice of filter values is imperfect (quite likely) or that the $dMLT$ parameter is itself inadequate to fully capture the convection cell behaviour (also quite likely).

To investigate the latter, we further probed the local time distributions of the dawn and dusk convection cell foci in Figure 4. An offset to the distribution corresponding to a clockwise rotation was noted, that might be partly responsible for the differing behaviour of the dawn and dusk foci mentioned above. Furthermore, we should note that this also implies a discrepancy between any discussion of dayside or nightside foci, and the use of $dMLT < 0$ or $dMLT > 0$, since any rotation could move both cell foci between the dayside and nightside without any change to $dMLT$. One factor known to introduce a clockwise rotation to the convection pattern is IMF $B_Y > 0$ (e.g. Grocott et al., 2012). Figure 1f revealed a B_Y-dependence of the foci locations, but an opposite one at dawn and dusk, thus corresponding to a rotation rather than a shift of both foci towards the dayside or nightside. We checked whether the inherent clockwise rotation might be due to any bias in the prevalence of IMF B_Y in the intervals studied. We found that only 47% of the intervals had $B_Y > 0$ and 53% had $B_Y < 0$, suggesting that the observed average clockwise rotation not due to IMF B_Y. This is also consistent with the findings of Grocott et al. (2012) who found a similar B_Y-independent clockwise rotation. To check for any significance to the potential bias in the dawn and dusk foci locations we can turn to Figure 4b-c. Here we showed the distributions of the foci local times for the dayside and nightside reconnection driven subsets separately. Whilst there is some spread in each case, the two subsets barely overlap, suggesting that they represent distinct populations.

We finally return briefly to the transpolar voltage data presented in Figure 3a. It was shown above that V_{PC} peaks occur at $dMLT$ values of ~ 11 h and ~ 13 h. That there is a local minimum at 12 h is consistent with a steady state of balanced dayside and nightside reconnection being less common than a dominance of either dayside or nightside driving. That the peak V_{PC} values decrease away from $dMLT = 12$ h, where we expect more dominant day or nightside driving is also consistent with the ECPC model. According to Lockwood (1991) V_{PC} is related to the dayside and nightside reconnection rates, V_D and V_N, by

$$V_{PC} = \frac{V_D + V_N}{2} \tag{1}$$

such that, for the case where either V_D or V_N is zero, V_{PC} is equal to half of the rate of the active reconnection line. If we assume that the most extreme $dMLT$ values correspond to the most imbalanced reconnection, then we might expect V_{PC} to be approximately half its peak value at these extremes.

5 Conclusions

In this paper we have presented an analysis of the locations of the foci of the twin-vortex ionospheric convection cells using a 20 year archive of SuperDARN radar obser-

vations. We filtered the data to include only intervals of particularly high backscatter echoes ($n > 250$) and also only intervals where the negative cell focus was constrained to $12-24$ MLT and the positive cell focus to $0-12$ MLT, consistent with Dungey cycle twin-vortex flow. We can conclude that the SuperDARN convection maps capture a wide spread of foci locations and that the locations are sensitive to both IMF B_Z and the AL index. This suggests that the cell foci locations are responding to differing rates of dayside and nightside reconnection. We further filtered the data by suitable ranges of B_Z and AL to isolate one population that is dominated by dayside reconnection and another dominated by nightside reconnection. Analysis of these data provides evidence that the response is consistent with the predictions of the expanding-contracting polar cap model. First, the foci tend to cluster at higher latitudes when dayside reconnection dominates, and lower latitudes when nightside reconnection dominates. Second, the hour angle between the dawn and dusk foci, $dMLT$, is reduced (foci closer to noon) when dayside reconnection dominates, and increases (foci closer to midnight) when nightside reconnection dominates.

We draw a number of further conclusions. The relationship between the foci local times and the AL index is not straightforward. Whilst we find that, at a fixed level of AL, $dMLT$ decreases with increasingly negative IMF B_Z we find that, at a fixed level of IMF B_Z, $dMLT$ increases with increasingly negative AL only up to modest values of AL (to ~ -200 nT). As AL becomes further enhanced $dMLT$ decreases again. We attribute this to an inherent dependence of AL on IMF B_Z in that, for AL to reach strongly negative values, B_Z must also be negative. In other words, episodes of intense nightside reconnection (and associated open flux closure) only occur if there has been, and is likely ongoing, persistent dayside reconnection (and open flux production). Only for relatively modest levels of dayside reconnection can nightside reconnection dominate. This interdependency complicates efforts to isolate the nightside component of the flow. The dayside component is easier to isolate, as it takes some time for nightside reconnection to become enhanced following the onset of dayside reconnection.

6 Open Research

SuperDARN data was accessed via the British Antarctic Survey data archive (https://www.bas.ac.uk/projec
Other data mirrors are hosted by the Virginia Tech SuperDARN group (http://vt.superdarn.org/) and the University of Saskatchewan (https://superdarn.ca/data-download). The radar data fitting and spherical harmonic analysis were performed using the FITACF2.5 library and version 4.2 of the Radar Software Toolkit (RST) (SuperDARN Data Analysis Working Group et al., 2018). The Map Potential data processing is described fully in (Walach et al., 2022) and we use the equivalent of their 'D4' dataset. All solar wind data were downloaded from NASA's SPDF Coordinated Data Analysis Web (https://cdaweb.gsfc.nasa.gov/index.html/). The AL auroral electrojet index used in this paper was provided by the WDC for Geomagnetism, Kyoto (http://wdc.kugi.kyoto-u.ac.jp/wdc/Sec3.html) (World Data Center for Geomagnetism, Kyoto et al., 2015).

Acknowledgments

The authors acknowledge the use of SuperDARN data. SuperDARN is a collection of radars funded by national scientific funding agencies of Australia, Canada, China, France, Italy, Japan, Norway, South Africa, United Kingdom, and United States of America, and we thank the international PI team for providing the data. A. Grocott and M.-T. Walach were supported by Natural Environment Research Council (NERC), UK, grant nos. NE/T000937/1 and NE/V00283X/1. S. Milan was supported by the Science and Technology Facilities Council (STFC), UK, grant no. ST/W00089X/1.

References

Borovsky, J. E., Hesse, M., Birn, J., & Kuznetsova, M. M. (2008). What determines the reconnection rate at the dayside magnetosphere? *Journal of Geophysical Research: Space Physics*, *113*(A7). Retrieved from https://agupubs.onlinelibrary.wiley.com/doi/abs/10.1029/2007JA012645 doi: https://doi.org/10.1029/2007JA012645

Boyle, C. B., Reiff, P. H., & Hairston, M. R. (1997, January). Empirical polar cap potentials. *J. Geophys. Res.*, *102*(A1), 111-125.

Chisham, G., Lester, M., Milan, S. E., Freeman, M. P., Bristow, W. A., Grocott, A., ... Walker, A. D. M. (2007, January). A decade of the Super Dual Auroral Radar Network (SuperDARN): scientific achievements, new techniques and future directions. *Surveys in Geophysics*, *28*, 33-109. doi: 10.1007/s10712-007-9017-8

Cowley, S. W. H., & Lockwood, M. (1992, February). Excitation and decay of solar wind-driven flows in the magnetosphere-ionosphere system. *Ann. Geophysicae*, *10*, 103-115.

Coxon, J. C., Milan, S. E., Clausen, L. B. N., Anderson, B. J., & Korth, H. (2014). A superposed epoch analysis of the regions 1 and 2 birkeland currents observed by ampere during substorms. *Journal of Geophysical Research: Space Physics*, *119*(12), 9834-9846. Retrieved from https://agupubs.onlinelibrary.wiley.com/doi/abs/10.1002/2014JA020500 doi: https://doi.org/10.1002/2014JA020500

Davis, T. N., & Sugiura, M. (1966). Auroral electrojet activity index ae and its universal time variations. *J. Geophys. Res.*, *71*(785).

Etemadi, A., Cowley, S. W. H., Lockwood, M., Bromage, B. J. I., Willis, D. M., & Luhr, H. (1988, May). The dependence of high-latitude dayside ionospheric flows on the north south component of the IMF - a high time resolution correlation-analysis using EISCAT POLAR and AMPTE UKS and IRM data. *Planet. Space Sci.*, *36*(5), 471-498.

Feldstein, Y. I., & Starkov, G. V. (1967). Dynamics of auroral belt and polar geomagnetic disturbances. *Planet. Space Sci.*, *18*, 401-454.

Fogg, A. R., Lester, M., Yeoman, T. K., Burrell, A. G., Imber, S. M., Milan, S. E., ... Anderson, B. J. (2020, MAY). An improved estimation of superdarn heppner-maynard boundaries using ampere data. *JOURNAL OF GEOPHYSICAL RESEARCH-SPACE PHYSICS*, *125*(5). doi: 10.1029/2019JA027218

Freeman, M. P., & Morley, S. K. (2004). A minimal substorm model that explains the observed statistical distribution of times between substorms. *Geophysical Research Letters*, *31*(12). Retrieved from https://agupubs.onlinelibrary.wiley.com/doi/abs/10.1029/2004GL019989 doi: https://doi.org/10.1029/2004GL019989

Gordeev, E. I., Sergeev, V. A., Pulkkinen, T. I., & Palmroth, M. (2011). Contribution of magnetotail reconnection to the cross-polar cap electric potential drop. *Journal of Geophysical Research: Space Physics*, *116*(A8). Retrieved from https://agupubs.onlinelibrary.wiley.com/doi/abs/10.1029/2011JA016609 doi: https://doi.org/10.1029/2011JA016609

Greenwald, R. A., Baker, K. B., Dudeney, J. R., Pinnock, M., Jones, T. B., Thomas, E. C., ... Yamagishi, H. (1995, February). Darn/SuperDarn: A global view of the dynamics of high-latitude convection. *Space Sci. Rev.*, *71*, 761-796. doi: 10.1007/BF00751350

Greenwald, R. A., Ruohoniemi, J. M., Baker, K. B., Bristow, W. A., Sofko, G. J., Villain, J.-P., ... Slavin, J. A. (1999). Convective response to a transient increase in dayside reconnection. *Journal of Geophysical Research: Space Physics*, *104*(A5), 10007-10015. Retrieved from https://agupubs.onlinelibrary.wiley.com/doi/abs/10.1029/98JA02723 doi: https://doi.org/10.1029/98JA02723

Greenwald, R. A., Ruohoniemi, J. M., Bristow, W. A., Sofko, G. J., Villain, J.-P., Huuskonen, A., ... Frank, L. A. (1996, October). Mesoscale dayside convection vortices and their relation to substorm phase. *J. Geophys. Res.*, *101*(A10), 21697-21713.

Grocott, A., Cowley, S. W. H., & Sigwarth, J. B. (2003, February). Ionospheric flow during extended intervals of northward but B_Y-dominated IMF. *Ann. Geophysicae*, *21*, 509-538.

Grocott, A., Cowley, S. W. H., Sigwarth, J. B., Watermann, J. F., & Yeoman, T. K. (2002, October). Excitation of twin-vortex flow in the nightside high-latitude ionosphere during an isolated substorm. *Ann. Geophysicae*, *20*, 1577-1601.

Grocott, A., Milan, S. E., Imber, S. M., Lester, M., & Yeoman, T. K. (2012). A quantitative deconstruction of the morphology of high-latitude ionospheric convection. *J. Geophys. Res.*, *117*(A5). Retrieved from `http://dx.doi.org/10.1029/2012JA017580` doi: 10.1029/2012JA017580

Grocott, A., Wild, J. A., Milan, S. E., & Yeoman, T. K. (2009). Superposed epoch analysis of the ionospheric convection evolution during substorms: onset latitude dependence. *Ann. Geophysicae*, *27*(2), 591-600.

Heppner, J. P., & Maynard, N. C. (1987, May). Empirical high-latitude electric-field models. *J. Geophys. Res.*, *92*(A5), 4467-4489.

Imber, S. M., Milan, S. E., & Lester, M. (2013). The Heppner-Maynard Boundary measured by SuperDARN as a proxy for the latitude of the auroral oval. *J. Geophys. Res.*, *118*(2), 685-697. doi: 10.1029/2012JA018222

Iyemori, T. (1990). Storm-time magnetospheric currents inferred from mid-latitude geomagnetic field variations. *Journal of geomagnetism and geoelectricity*, *42*(11), 1249-1265. doi: 10.5636/jgg.42.1249

Lockwood, M. (1991). On flow reversal boundaries and transpolar voltage in average models of high-latitude convection. *Planetary and Space Science*, *39*(3), 397–409.

Lockwood, M., Lanchester, B. S., Morley, S. K., Throp, K., Milan, S. E., Lester, M., & Frey, H. U. (2006). Modeling the observed proton aurora and ionospheric convection responses to changes in the imf clock angle: 2. persistence of ionospheric convection. *Journal of Geophysical Research: Space Physics*, *111*(A2). Retrieved from `https://agupubs.onlinelibrary.wiley.com/doi/abs/10.1029/2003JA010307` doi: https://doi.org/10.1029/2003JA010307

Lockwood, M., & McWilliams, K. A. (2021, SEP). A survey of 25 years' transpolar voltage data from the superdarn radar network and the expanding-contracting polar cap model. *JOURNAL OF GEOPHYSICAL RESEARCH-SPACE PHYSICS*, *126*(9). doi: 10.1029/2021JA029554

Lockwood, M., & Morley, S. K. (2004). A numerical model of the ionospheric signatures of time-varying magnetic reconnection: I. ionospheric convection. *Ann. Geophys.*, *22*(1), 73–91.

MacDougall, J. W., & Jayachandran, P. T. (2001). Polar cap convection relationships with solar wind. *Radio Science*, *36*(6), 1869-1880. Retrieved from `https://agupubs.onlinelibrary.wiley.com/doi/abs/10.1029/2001RS001007` doi: https://doi.org/10.1029/2001RS001007

Milan, S. E., Carter, J. A., Sangha, H., Bower, G. E., & Anderson, B. J. (2021). Magnetospheric flux throughput in the dungey cycle: Identification of convection state during 2010. *Journal of Geophysical Research: Space Physics*, *126*(2), e2020JA028437. Retrieved from `https://agupubs.onlinelibrary.wiley.com/doi/abs/10.1029/2020JA028437` (e2020JA028437 2020JA028437) doi: https://doi.org/10.1029/2020JA028437

Milan, S. E., Gosling, J. S., & Hubert, B. (2012, MAR 28). Relationship between interplanetary parameters and the magnetopause reconnection rate quantified from observations of the expanding polar cap [Article]. *J. Geophys. Res.*, *117*. doi: {10.1029/2011JA017082}

Milan, S. E., Grocott, A., de Larquier, S., Lester, M., Yeoman, T. K., Freeman, M. P., & Chisham, G. (2013). Travelling ionospheric disturbances in the Weddell Sea Anomaly associated with geomagetic activity. *J. Geophys. Res.*, *118*. doi: 10.1002/jgra.50566,

Milan, S. E., Grocott, A., Forsyth, C., Imber, S. M., Boakes, P. D., & Hubert, B. (2008, August). Looking through the oval window. *Astronomy and Geophysics*, *49*(4), 4.16-4.18. doi: 10.1111/j.1468-4004.2008.49416.x

Milan, S. E., Grocott, A., Forsyth, C., Imber, S. M., Boakes, P. D., & Hubert, B. (2009). A superposed epoch analysis of auroral evolution during substorm growth, onset and recovery: open magnetic flux control of substorm intensity. *Ann. Geophysicae*, *27*(2), 659-668.

Nakai, H., & Kamide, Y. (2003). Substorm-associated large-scale magnetic field changes in the magnetotail: a prerequisite for "magnetotail deflation" events. *Annales Geophysicae*, *21*(4), 869–879. Retrieved from `https://angeo.copernicus.org/articles/21/869/2003/` doi: 10.5194/angeo-21-869-2003

Ruohoniemi, J. M., & Baker, K. B. (1998, September). Large-scale imaging of high-latitude convection with Super Dual Auroral Radar Network HF radar observations. *J. Geophys. Res.*, *103*, 20797-20811. doi: 10.1029/98JA01288

Ruohoniemi, J. M., & Greenwald, R. A. (2005, September). Dependencies of high-latitude plasma convection: Consideration of interplanetary magnetic field, seasonal, and universal time factors in statistical patterns. *J. Geophys. Res.*, *110*(A9). doi: 10.1029/2004JA010815

Shepherd, S., & Ruohoniemi, J. (2000, October). Electrostatic potential patterns in the high-latitude ionosphere constrained by SuperDARN measurements. *J. Geophys. Res.*, *105*(A10), 23005-23014.

Smith, C. W., L'Heureux, J., Ness, N. F., Acuña, M. H., Burlaga, L. F., & Scheifele, J. (1998, July). The ACE magnetic fields experiment. *Space Sci. Rev.*, *86*, 613-632. doi: 10.1023/A:1005092216668

Sotirelis, T., Keller, M. R., Liou, K., Smith, D., Barnes, R. J., Talaat, E., & Baker, J. B. H. (2017). Testing the expanding-contracting polar cap paradigm. *Journal of Geophysical Research: Space Physics*, *122*(7), 7077-7086. Retrieved from `https://agupubs.onlinelibrary.wiley.com/doi/abs/10.1002/2017JA024238` doi: https://doi.org/10.1002/2017JA024238

Stone, E. C., Frandsen, A. M., Mewaldt, R. A., Christian, E. R., Margolies, D., Ormes, J. F., & Snow, F. (1998, July). The Advanced Composition Explorer. *Space Sci. Rev.*, *86*, 1-22. doi: 10.1023/A:1005082526237

SuperDARN Data Analysis Working Group, Thomas, E. G., Ponomarenko, P. V., Billett, D. D., Bland, E. C., Burrell, A. G., & Walach, M.-T. (2018). *Superdarn radar software toolkit (rst) (version 4.2) [software].* doi: 10.5281/zenodo.1403226

Thomas, E. G., & Shepherd, S. G. (2018, April). Statistical Patterns of Ionospheric Convection Derived From Mid-latitude, High-Latitude, and Polar SuperDARN HF Radar Observations. *J. Geophys. Res-Space Phys.*, *123*(4), 3196–3216. doi: 10.1002/2018JA025280

Walach, M.-T., & Grocott, A. (2019). Superdarn observations during geomagnetic storms, geomagnetically active times, and enhanced solar wind driving. *Journal of Geophysical Research: Space Physics*, *124*(7), 5828-5847. Retrieved from `https://agupubs.onlinelibrary.wiley.com/doi/abs/10.1029/2019JA026816` doi: https://doi.org/10.1029/2019JA026816

Walach, M.-T., Grocott, A., Staples, F., & Thomas, E. G. (2022). Super dual auroral radar network expansion and its influence on the derived ionospheric convection pattern. *Journal of Geophysical Research: Space Physics*, *127*(2), e2021JA029559. Retrieved from `https://agupubs.onlinelibrary.wiley.com/doi/abs/10.1029/2021JA029559` (e2021JA029559 2021JA029559) doi:

https://doi.org/10.1029/2021JA029559

Walach, M.-T., Milan, S. E., Yeoman, T. K., Hubert, B. A., & Hairston, M. R. (2017). Testing nowcasts of the ionospheric convection from the expanding and contracting polar cap model. *Space Weather*, *15*(4), 623-636. Retrieved from `https://agupubs.onlinelibrary.wiley.com/doi/abs/10.1002/2017SW001615` doi: https://doi.org/10.1002/2017SW001615

Weimer, D. R. (2005, May). Improved ionospheric electrodynamic models and application to calculating joule heating rates. *J. Geophys. Res-Space Phys.*, *110*(A5). doi: 10.1029/2004JA010884

World Data Center for Geomagnetism, Kyoto, Nose, M., Iyemori, T., Sugiura, M., & Kamei, T. (2015). *Geomagnetic ae index [dataset].* doi: 10.17593/15031-54800